Vehicle Description Form

Human Powered Vehicle Challenge 2011

(HPVC Form 6)

East Event Host: Rose-Hulman Institute of Technology, Indianapolis, IN. Apr 29-May 1, 2011

West Event Host: Montana State University, Bozeman, MT. May 13-15

http://www.asme.org/hpv

*** *This is a required document for <u>all</u> teams. Please incorporate it into your Design Report* ***

EAST
March 28, 2011

***
Please Observe Your Due Dates

WEST
April 11, 2011

Vehicle Description

Competition Location: _____

School name: _____

Vehicle name: _____

Vehicle number _____

Vehicle type   Unrestricted_____   Speed_____

Vehicle configuration

          Upright _____   Semi-recumbent _____

          Prone _____   Other (specify) _____

Frame material   _____

Fairing material(s)   _____

Number of wheels   _____

Vehicle Dimensions *(please use inches, pounds)*

          Length _____   Width _____

          Height _____   Wheelbase _____

Weight Distribution   Front _____   Rear _____   Total _____

Wheel Size   Front _____   Rear _____

Frontal area   _____

Steering   Front _____   Rear _____

Braking   Front _____   Rear _____   Both _____

Estimated Cd   _____

Vehicle history (e.g., has it competed before? where? when?)_____

_____

_____

_____

_____

_____

Design Report

Olin College Human Powered Vehicle

Shadowfax

Franklin W. Olin College of Engineering

Team Leaders: Travis Schuh and Ben Smith

Team Members: Charlie Behling, Andrew Carmedelle, Ben Chapman, Elsa Culler, Geetanjali Gubba, Jacob Izraelevitz, Eric Jones, Dan Kearney, Meghan Murray, Heidi Nafis, Alex Niswander, Juliana Nazare, Jackie Rose, John Rosenwinkel, Travis Schuh, Ben Smith, Orion Taylor

Table of Contents

Abstract

The Olin College Human Powered Vehicle Team is returning for its fifth ASME HPV Challenge. The main goals of this season are to improve reliability, speed potential, and manufacturing processes of the vehicle. As in past years, the vehicle is designed so all team members, regardless of athletic ability, height, and bike experience, are able to ride the bike effectively.

Improving upon last year's vehicle *Bucephalus*, the 2011 competition vehicle *Shadowfax* incorporates the following innovations:

1. With a focus on improved manufacturing techniques, *Shadowfax* exhibits improved reliability and quality with respect to *Bucephalus*. These improvements include an adjustable, custom frame jig to fully constrain the frame during welding and a well-researched, improved method for fairing fabrication that will reduce weight and improve overall tolerancing.
2. Significant component optimization in *Shadowfax* increases rider efficiency and comfort. A custom, woven fabric seat to decrease weight and allow for more universal adjustment, machined cranks and bottom bracket to minimize pedal path and decrease q-factor, and front and rear disc brakes for enhanced stopping performance are a few of the component-level optimizations added to our vehicle this year.
3. Substantial testing of *Shadowfax* has informed and supported our design decisions. Major experimentation of nonlinear steering and wheel positioning for specific rake and trail values, fiberglass and carbon composite sample strength testing, and drivetrain efficiency testing have allowed for direct justification of our design work.
4. Sophisticated analysis of the fairing using professional-grade Computational Fluid Dynamics software has allowed us to intelligently iterate fairing designs. We performed analysis with CD-adapco, a software package utilized by NASA, to compute accurate fluid flow on our fairing.

Overall, we hope that *Shadowfax* continues Olin College's trend of increased quality and competitiveness of each year's bicycle.

Design and Innovation

Frame Jig Fabrication

Before designing this year's prototype, we devoted time to the design and fabrication of a frame jig. Vehicles from previous years were plagued with chain derailments due to non-planar frames, which cost significant time during race events. A frame jig which constrained frame tubes such that they lie in a single plane eliminated such issues and saved us valuable time. Most bicycle manufacturers rely on rigid vertical frame jigs to hold tubes in plane. However, such a design is much less economical for the distributed layout of recumbent frames. Our jig used 80/20 aluminum extrusion as a base, and had smaller, sliding, adjustable segments which held the frame tubes in their proper places. To hold the main frame tubes in one plane, a c-channel is spaced above the sliding segments of 80/20 on which the frame tubes can be clamped.

Equally important as the frame tubes being coplanar was for the frame components (the head tube, bottom brackets and wheel axles) to be normal to the main frame plane. To accomplish this, we fabricated devices to center each of these components about the frame. Before welding, the frame jig was laid atop a printout of the frame and the component of interest was aligned vertically above the printout. The tubes and components were then tack welded, removed from the jig, and welded fully.

Unlike a number of our previous bikes, the prototype, *Bilius*, could be consistently backpedaled, indicating successful chain alignment. We did find some misalignment problems that arose from welding the frame after removing it from the jig. To minimize these problems, we tacked components on all sides before removal from the jig. The increased time associated with creating and using the frame jig was worth the increased efficiency as a result of the decrease in drivetrain difficulties.
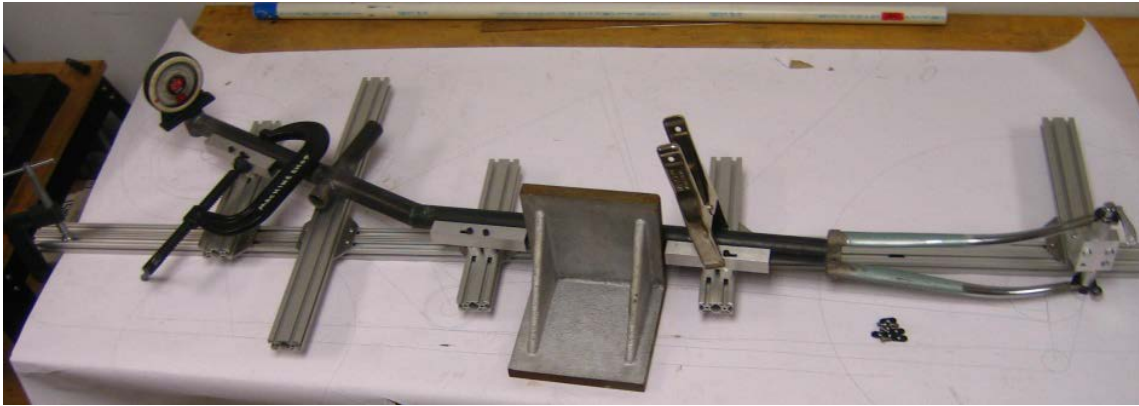
Figure 1: Frame Jig. Frame of prototype *Bilius* held in jig prior to welding.

Nonlinear Steering Design

When considering the design of our steering system, we worked to optimize rider comfort while taking advantage of open space in *Shadowfax's* layout so as not to increase our frontal area. Early in the design process we decided to place the handlebars above the frame, rather than under it as in last year's competition vehicle.

On a recumbent vehicle, the steering column tends to be far in front of the ideal handlebar location. To avoid unnecessary tiller, the handlebar and steering axes must be separated and connected via a mechanical linkage. A separation of axes allows for a varying ratio between steering input angle and steering rotation: that is, the steering can be made more or less sensitive by changing the size and shape of the input and output linkages. Low sensitivity is desired at high speeds, where aggressive steering motions produce dangerous maneuvering. However, at low speeds and winding courses, high sensitivity is desired in order to make sharp turns and corrections. A nonlinear steering ratio is therefore ideal as it combines both qualities: low sensitivity for small input angles and high sensitivity for large angles.

Quantitatively, we decided that the ideal steering system would yield an equal steering angle and wheel angle at high but still comfortable driver input angles. At small angles, we want a steering ratio of about 2:1, and we want a smooth transition between low and high sensitivity steering. We suspected that a pair of elliptical cams could accomplish this. As a test, we made a MATLAB simulation that allowed us roughly estimate the changing input-to-output ratio as one ellipse rotated another. We then made a physical model and tested our predictions. Our final prototype used steel wires running over cams that are sandwiched such that the wire is confined to a narrow middle ellipse between two larger ones. As the CAD in Figure 2 shows, the handlebar ellipse is larger and more eccentric than the output ellipse connected to the fork.
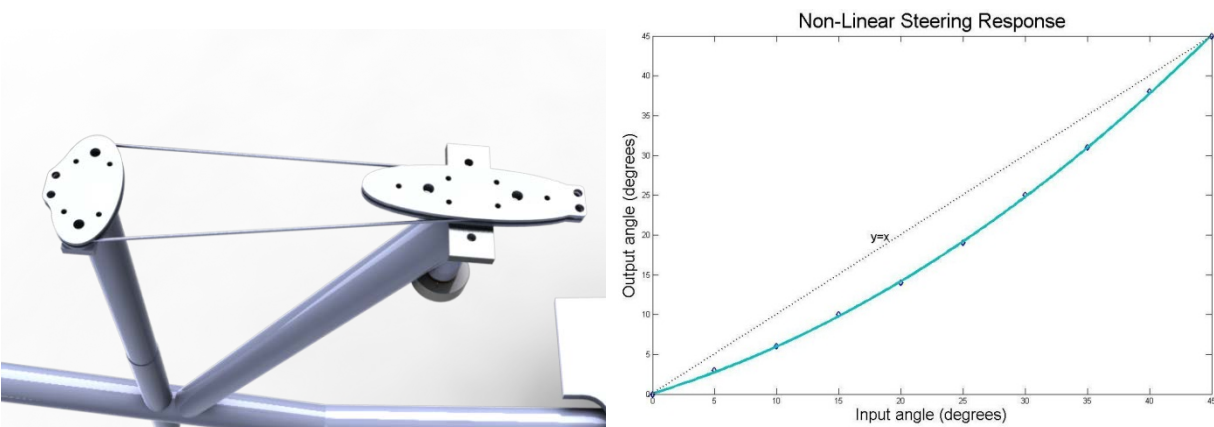

Figure 2: Nonlinear Steering Ellipses and Response. Ellipses mounted on handlebar post and steering column provided nonlinear steering effects. The teal line shows a MATLAB plot of the angular displacement of the steering column as a result of rotating the handlebars.

These ellipses provide the steering response curve also seen in Figure 2. Starting at 0°, the steering has an insensitive 2:1 response until about 10°, after which it smoothly catches up to the final ratio of 1:1 at 45°. This combination of ellipses achieved our desired sensitivity goals.

After extensive revision of this steering geometry and testing in reference to a traditional four-bar linear steering configuration, we compared the two designs in a design matrix shown in Table 1. Based on the design matrix, we decided that linear steering is the most advantageous, because while linear steering is very unique and innovative, we did not find enough of a difference in performance to justify the reduction in robustness and safety.

STEERING DESIGN MATRIX		
Criteria	*Linear Steering*	*Nonlinear Steering*
Innovation	1	2
Robustness	2	1
Control	1.5	1.5
Manufacturability	2	1
Safety	2	1
TOTAL	8.5	6.5

Table 1: Design Matrix for *Shadowfax's* Steering. Note that a rating of 2 is better than 1. Control was made the same across both steering because we did not find a noticeable performance difference in testing.

Seat Design

The seat design goals included decreasing the weight from past years' designs and maintaining the team's commitment to all team members being able to comfortably ride the bike. During initial brainstorming, we came up with three seat designs – a wooden seat as with previous years, a composite carbon fiber seat, and a steel framed hammock seat. In order to decide between designs, we compared them in the design matrix seen in Table 2. In order to reduce weight, *Shadowfax's* seat design moved from a solid seat bottom and back made of plywood to the steel frame hammock design as shown in Figure 3. This change reduces the seat assembly weight from 5.2kg to 3kg, a 42% reduction.

SEAT DESIGN MATRIX			
Criteria	*CARBON FIBER*	*WOVEN*	*WOOD*
Comfort	2	3	1
Power Transfer Efficiency	3	1	2
Adjustability (2x weight)	1	3	2
Innovation	2	3	1
Weight (2x weight)	3	2	1
Manufacturability (2x weight)	1	2	3
TOTAL	17	22	15

Table 2: Design Matrix for *Shadowfax's* seat. Note that a rating of 1 is worst and 3 is best. Manufacturability, Weight, and Adjustability were give 2x weight because they were our top priorities.

We made the test weave to that the polypropylene was strong enough to support our riders. From this, we determined that the test weave remained approximately rigid with the rider weight, and that using a polypropylene weave instead of a rigid wooden seat will not significantly reduce power transfer to the bike.

Figure 3: CAD Seat Model and Manufactured Seat. The triangular linkage system on the seat back provides an adjustable seat angle and rails allow for positional changes. A hammock woven across the steel frame to provides the rider a lightweight seat. The weaving is backed with foam padding for added comfort.

The seat's most unique innovation is its adjustable seat back (Figure 3). The seat back tilts between 35⁰ and 55⁰ above horizontal, allowing our entire rider set to see out the window. This is accomplished by a triangular linkage with the seat back. One corner of the triangle is fixed to the seat back, one rests on the main tube, and the third is pinned into one of several holes on the seat back. The seat angle can therefore be modified by relocating the pinned corner. The seat can also be moved forward and backwards by relocating the pins on the seat bottom, sliding the seat along two rails.

Drivetrain Design

When designing our drivetrain, we arrived at the realization that frontal area can be minimized if the space behind the rider's footpath is fully utilized. To that end, we designed the drivetrain to fit behind the heel's lowest point and the toe's highest position. The drivetrain on *Shadowfax* can be seen in Figure 4. After analysis, we found a configuration that allowed the entire drivetrain and rider to fit behind the pedal path. This discovery validated our design decision to run rear wheel drive on the bike. We previously felt that front wheel drive reduced our frontal area by enough to overcome its efficiency losses. However, *Shadowfax's* rear wheel drive configuration is, based on testing shown in *Drivetrain Performance Testing*, more efficient than front wheel drive and does not significantly increase the bike's frontal area.
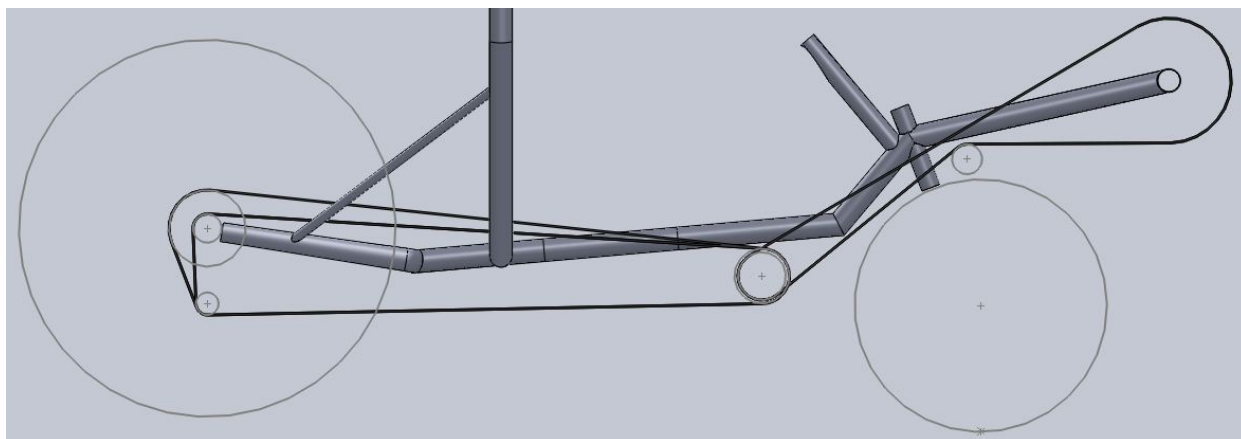

Figure 4: Drivetrain Path on *Shadowfax*. The black lines show the chain path for *Shadowfax's* drivetrain. Both the highest and lowest gear paths are shown from the back wheel to the interchange.

Custom Crank Arms

In order to reduce the width and height of our bike's nose, we designed a custom crankset and bottom bracket. To fabricate the bottom bracket, we narrowed a standard bottom bracket sleeve from 69mm to 43mm and rethreaded one side of the sleeve. This narrower bottom bracket required the use of bearing cups rather than a standard cartridge bottom bracket.

Figure 5: Custom Crank Comparison. Note custom narrower bracket and custom flat cranks on the prototype vehicle to the left. These changes narrow the footpath by 2.75in.

We then fitted this narrower bottom bracket with custom billet aluminum cranks. Whereas standard cranks flare out to allow chainstay clearance, we did not have to worry about interference and machined planar cranks, further reducing the crank tread or distance between the rider's feet. A comparison of our custom cranks with standard bicycle cranks can be seen in Figure 5. We were able to reduce the q-factor from 6.75in for conventional cranks to 4in on the prototype vehicle and then 3.75in for *Shadowfax*.

To determine an appropriate crank length that improves our aerodynamics without compromising rider power, we placed pedal mount holes in *Bilius's* crank arms at both 135mm and 175mm for rider testing. Riders found that both lengths were easy to adapt to, consistent with the observations in [1]. However, the longer arms allowed the riders to transfer more torque when starting the vehicle, so most riders preferred the longer cranks. As a compromise, we opted for 160mm cranks on *Shadowfax*, obtaining a slight aerodynamic gain. Finite element analysis validating the strength of the crank arms can be seen in Figure 13.

Though narrowing the bike's tread does not decrease its total frontal area, it does allow for a fairing with a more gradual transition from its front-most point to the roll bar. Also, reducing the distance between the pedals allows for a more natural pedaling position and eliminates the need for riders to bow their legs out unnecessarily.

Gear Ratio Design

Our target top speed for the bike is approximately 35 mph. In order to pick gear ratios, we created a spreadsheet that predicts the bike speed given the sprocket sizes, drive wheel size, and rider cadences (Table 3).

We referenced the power vs. cadence revolutions per minute curve in *Bicycling Science* [2] to obtain the maximum cadence for forward pedaling. The maximum occurs at approximately 85 rpm. However, we scaled up the maximum cadence to account for our shorter cranks. Thus, we have 90.31 rpm as our medium cadence value, and we approximated 15 rpm above and below the medium value to obtain a high cadence of 106 rpm and a low cadence of 74 rpm. This puts our optimum speed at approximately 34.7 mph. Our final top speed at max cadence in the highest gear is predicted to be at 41mph and our slowest speed at low cadence in the lowest gear is predicted to be at 10.5 mph. We chose to use a standard 8-speed cassette and a 22T to 20T interchange combination in order to minimize the height our chain path adds to the bike. Based on these constraints, we picked a ratio for the first reduction to achieve our design goal. We wanted to be sure that our cassette has a fine resolution of gears in the high range so that we will be able to optimize our rider cadence at speed.

DRIVETRAIN SPECIFICATION			CASSETTE	RATIO	LOW SPEED (mph)	MID SPEED (mph)	HIGH SPEED (mph)
Chain Ring	53	teeth	30 T	1.94	10.53	12.78	15.04
Interchange 1	20	teeth	26 T	2.24	12.15	14.75	17.35
Interchange 2	22	teeth	23 T	2.53	13.73	16.67	19.61
Wheel Diameter	24.48	inch	20 T	2.92	15.79	19.17	22.56
Crank Length	160	mm	17 T	3.43	18.58	22.56	26.54
Low Cadence	74.38	rpm	15 T	3.89	21.05	25.56	30.07
Medium Cadence	90.31	rpm	13 T	4.48	24.29	29.50	34.70
High Cadence	106.3	rpm	11 T	5.30	28.71	34.86	41.01

Table 3: Relative speeds (in mph) for each gear in the cassette.

Alternative Derailleur Configuration

In order to reduce the height of our fairing, we experimented with an alternate derailleur configuration. The slack chain line defines the bottom edge of our fairing, so raising this chain line could reduce our frontal area. To do this, we rotated the derailleur towards the rear fork blade on a new mounting tab. A comparison of the normal and alternate configurations can be seen in Figure 6. This eliminates the derailleur's ability to tension the chain, but it still successfully shifts. We then added a tensioner near our interchange to take up extra slack in the chain. After implementation, we realized that that the new configuration reduces the chain's height by such a small amount that reductions in air drag would be nullified by increased drivetrain losses from the added tensioning gears.
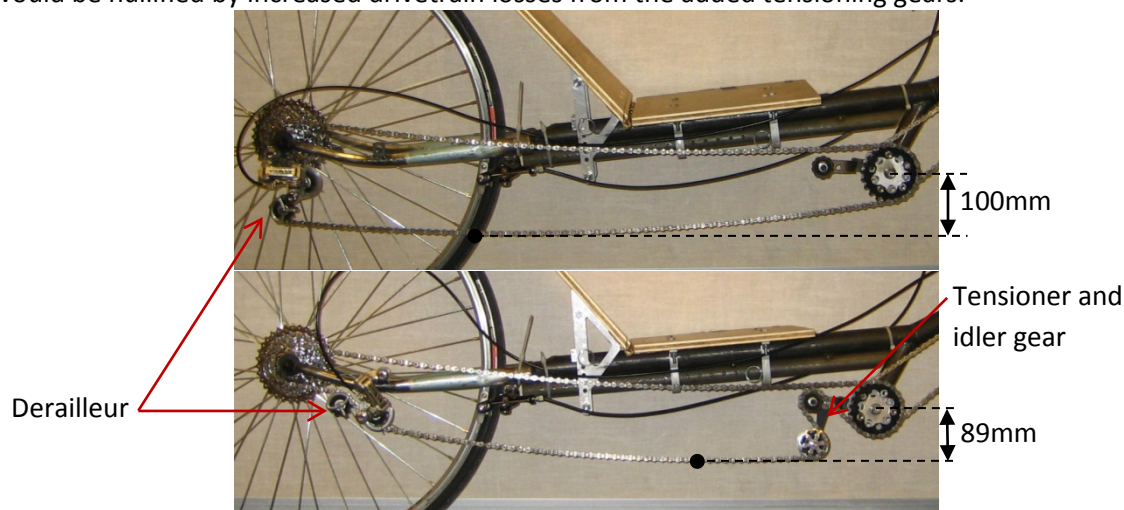

Figure 6: Alternate Derailleur Configuration. Despite decreasing the height of the fairing by 11mm, the gains from rotating the derailleur are likely negligible in comparison to drivetrain losses around the added idler and tensioner pulley.

Fairing Shape Design

One important consideration for our bike design was ensuring that all members of our team can ride the bicycle. This is not a new goal, but we approached it differently than in the past. With a range of heights and other dimensions of possible riders, it is challenging to build a bike that can be ridden quickly and efficiently by many differently sized people. To tackle this design problem, we first measured our team members. This year, we measured more accurately because we simulated the riding position instead of measuring while sitting normally or standing. Pedals were mounted on a piece of plywood and the seat from last year's bike *Bucephalus* was placed on the ground with a large piece of paper behind to mark riders' profiles (Figure 7). We recorded parameters—seat location, height of knees, top of head with helmet, eye level, and others—for many members of the team in their most comfortable riding position. From these measurements, we created a point cloud to represent each rider in the CAD model and designed the frame, seat, roll bar, and fairing to encompass these points.

Figure 7: Rider Measurement. From this setup we were able to make a complete rider profile on which to base our fairing shape.

The roll bar must protect all riders, but we also strive to minimize the roll bar in order to also minimize the frontal area. The roll bar is an important safety feature, so to size it properly we printed out a scale model which we fit over riders in order to validate the design prior to welding.

Based on the individual measurements and the vehicle CAD, we determined the location of each rider's eyes. From this, the fairing was designed with a window large enough that all riders can see straight out without the added difficulty of a shallow window angle.

Mold Manufacture

Over the past few years we have experimented with different methods of mold fabrication for the fairing. Last year's mold was made using a fabricated cloth skin supported from the inside by a weather balloon. We were unhappy with the results from this method as the fairing "ballooned out" on the sides and did not give us the sleek profile that we had intended. Our previous troubles in fairing construction merited the extra experimentation we performed for *Shadowfax's* mold.

This year we wanted to use a more robust mold and we tried a number of methods using ⅓-scale models of the fairing. Our first model consisted of a corrugated cardboard skeleton made using cross-sections from the fairing CAD. In the spaces between the "ribs" we used cardboard partitions and spray-foam to create an outer surface. This method proved unsatisfactory as it was too difficult to get a smooth surface using the spray foam. Even after sanding, the surface was full of pits caused by bubbles in the foam. To get a satisfactory surface, we would have had to cover the mold with BONDO, adding to the already-high price spray foam.

The second method we tried involved a similar skeleton of 1" expanded polystyrene (XPS) foam and a "skin" made of strips of ⅜" XPS foam screwed to the skeleton. This, with the addition of a solid foam nose cone, provided a mold with a satisfactorily smooth finish. Unfortunately, when we performed a layup on this mold, the force from the vacuum bagging caved in the suspended sections as seen in Figure 8. This would be even more of a problem on a full-scale version. Our pump pulls a vacuum of 18" of mercury, which equates to an unreasonable 88 pounds on a 1" x 10" span in the full-scale mold.
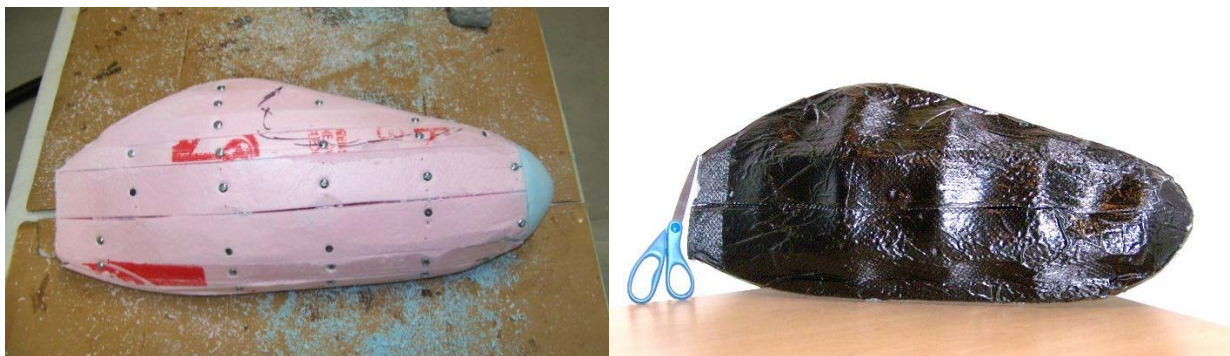

Figure 8: Hollow Model Fairing Mold and Layup Result. Foam skeletal structure covered with thin strips of 3/8" foam (left). After layup and vacuum-bagging, the pressure from the atmosphere collapsed the space between our ribs creating large indentations in the part.

Our full scale mold will consist of a solid foam body smoothed by body filler. This is the most robust solution and should give us very precise control over the finished fairing shape. For this, we will use cross-sections cut from 2" XPS foam and glue them together to form our final shape. We will sand the shape to get the profile and surface finish we want before the lay-up and vacuum bagging.

Layup Technique

This year, rather than using a traditional layup method, we invested in vacuum bagging equipment. This process, which removes air from a sealed bag containing the mold and final fairing, uses atmospheric pressure to compress the epoxy and layers of fiber during the curing process. Even more significant, an absorbent layer of cloth outside the fairing pulls excess epoxy from the fiber matrix, reducing the weight and improving the cohesion between layers of fiber. Epoxy adds brittle layers to the final composite. These layers add considerably less strength for their weight than do layers of fiber. Estimated weights of a completed fairing using different materials and techniques can be seen in Table 4.

Material and Layup Method	Estimated Fairing Weight (kg)
Standard Carbon	6.457
Vacuum-Bagged Carbon	4.862
Standard Fiberglass	6.094
Vacuum-Bagged Fiberglass	4.598

Table 4: Fairing Weight Analysis. Predicted weights of 2010 bike *Bucephalus*'s fairing (Surface Area = 5.67 m^2). Estimate approximates fairing as shell with two layers of fiber and no window.

Using fiberglass as opposed to carbon fiber saves 6% in the total fairing's weight; the design decision not to use fiberglass is discussed under Fairing Material Testing. However, using vacuum bagging as opposed to standard layup methods provides a 25% weight reduction regardless of the material chosen. For this reason and for reasons discussed under Fairing Material Testing, we will be vacuum-bagging our final fairing.

Analysis

Frame Analysis

To analyze the structural strength of the frame, we want to confirm that the frame geometry is able to withstand forces at a range of frequencies as would be observed from riding over rough conditions. Ideally, we would perform a dynamic harmonic analysis of the frame in order to observe the frame's response to a complete range of frequencies and to confirm that the bike will not fail when excited at its resonance frequency. Unfortunately, the FEA analysis techniques available to us do not provide a way to accurately set up the boundary conditions and thus do not give us usable results. However, we were able to identify the natural frequencies of the frame in comparison to frequencies that we observed during testing. We were able to approximate the dynamic loading with static loading of a rider through a 3g bump and a 0.75g braking force acting through the center of mass of the vehicle.

It is an industry standard to analyze bike frame strength by fixing the frame at the dropouts and then load the frame with three times the riders weight to simulate a bump of 3g [3]. The maximum braking force that the bike can experience is limited by the static coefficient of the tires, and thus a coefficient of friction of 0.85 [4] limits the braking force to a 0.85g braking force. We used a rider weight of 160lbf, which is our largest rider weight. When applied in combination, these two forces represent the worst case loading scenario that we expect to see through regular riding in competition.

These two forces were then applied through the center of mass of the bike and rider. We approximated the center of mass of the rider based on average seating position and calculated the center of mass of the bike based on the SolidWorks model. To constrain the front drop out, we approximated the fork as a continuation of the head tube going to the center of the wheel and constrained at the end point. We then constrained the rear dropout so that it was fixed in all directions except for along the direction of travel in order to represent the allowance for flex in the frame.
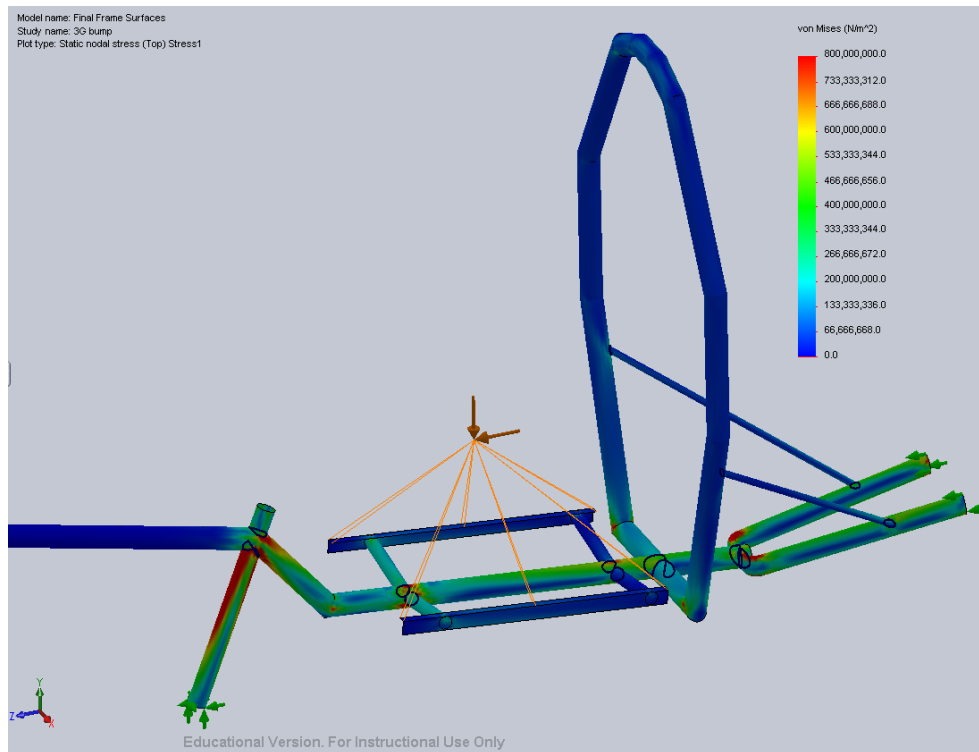
Figure 9: Analysis of frame with 3G bump and 1G braking force. This figure shows the effective von Mises stress. The yield strength of 4130 steel tubing is 460MPa.

When we analyzed the frame using SolidWorks's static FEA package (Figure 9), we found the effective von Mises stress to be under the yield strength except at the boundary conditions and joints, which is likely due to an artifact of the FEA and not our design (see roll bar analysis section for more explanation). Based on our frame withstanding this extreme loading condition, we are confident that our frame will be strong enough through the loading that it will experience during use.

In addition to analyzing the static response of the frame, we analyzed the frame for the natural frequencies of the frame with no constraints. The first 6 nonzero resonant frequencies are 8.4259Hz, 9.0347Hz, 13.995Hz, 26.857Hz, 40.053Hz, and 55.202Hz. We then compared these natural frequencies to data collected in the previous year of the frequency content observed while riding a bike over a bump. In both cases, there is a natural frequency around 20 Hz and the frequency testing confirms that these natural frequencies will be excited. Based on this, we can see that it would be valuable to analyze loading at these frequencies. This is an area for future development that would be valuable to find the resources for and invest the time in learning.

Fairing Analysis

The fairing analysis aimed to evaluate an initial fairing and use that to iterate to a more aerodynamic model. To this end, we used CD-adapco's STAR-CCM+ CFD software to analyze different fairing designs. In the past we performed our analysis in SolidWorks Flow Simulation or COSMOS FloWorks, but this year we prioritized acquiring full-fledged CFD software to add more credibility to our analysis. Our analysis with STAR-CCM+ is much more comprehensive, enabling us to better understand the fluid dynamics inherent to each fairing.

As stated in *Fairing Shape Design*, we built the initial fairing to fully encompass our rider and vehicle. From this preliminary model we derived two other configurations that could potentially increase our performance. As shown in Figure 10, Iterations 2 and 3 had less rear curvature and a rear wheel box, respectively. For comparison, the bottom right fairing is that of *Bucephalus*, our 2010 race vehicle.
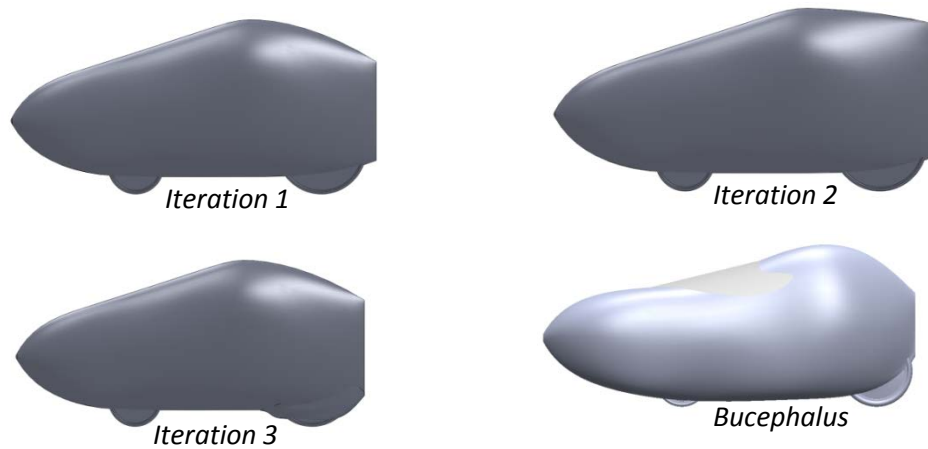
Figure 10: Fairing Shape Iterations. Note that *Bucephalus* has a lower profile than the current candidates.

To calculate flow trajectories, we assumed a vehicle speed of 30mph. We ran two simulations on each possible fairing: one assuming no external wind conditions, and one with a 10.4 mph [5] perpendicular crosswind. We included a ground moving at 30mph under the vehicle. In past analysis we neglected the ground, incorrectly deflating the drag force by reducing the constraints on the fluid flow. In addition, this year we included the wheels in our analysis as solid bodies, which well-represent the wheel discs we plan to put on our vehicle.

In the initial analysis, we computed the fluid velocity profiles and subsequent drag force on each fairing in STAR-CCM+ (Figure 11). As shown, *Bucephalus* has a larger stagnation region from increased flow separation around the fairing. Iterations 2 and 3 exhibit small stagnation flow regions as a result of their low overall curvature. The fact that *Bucephalus's* drag force is much higher than Iterations 2 or 3 (Table 5) is supported by the flow trajectories.
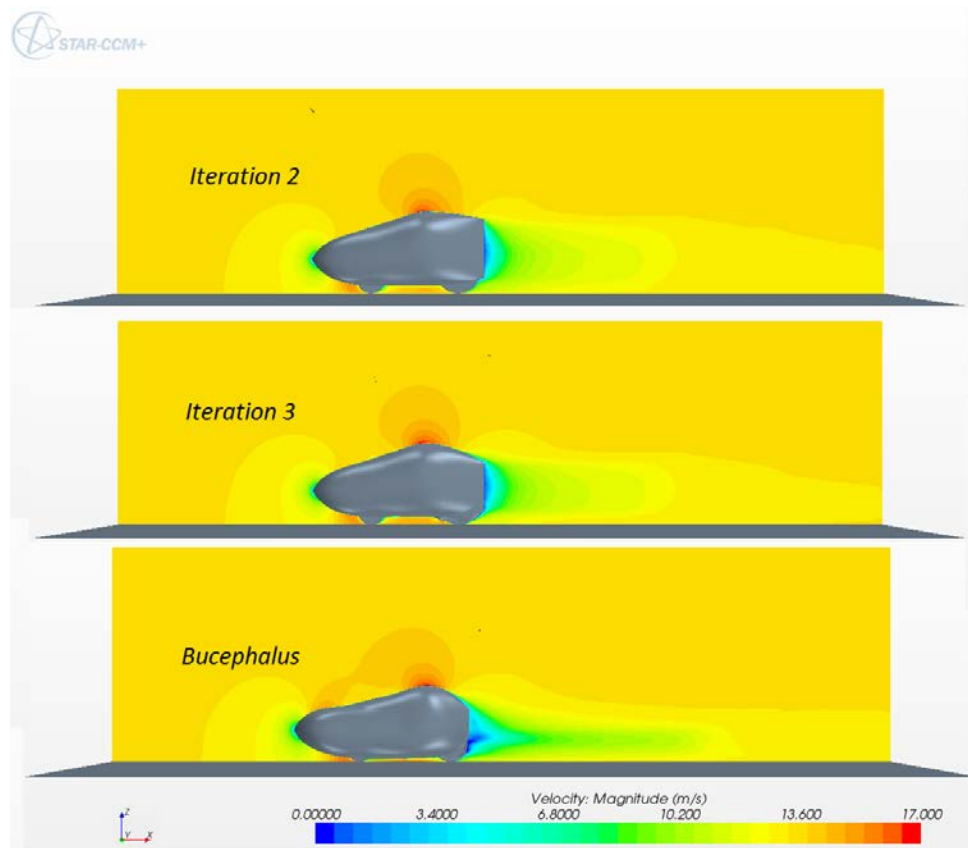

Figure 11: Fluid Velocity Profiles for Selected Fairing Iterations. Note that *Bucephalus* has a much larger area of stagnation behind the fairing, while Iteration 2 and 3 have smaller stagnation regions.

Since the fairing performance depends on low drag force, which in turn is a function of geometric and fluid parameters, we can compare our fairings via the metric of C$_d$A (drag coefficient times area):

$$C_d A = \frac{2F_D}{\rho v^2}$$

Taking our numerically computed value of F_D, density of air to be $1.2\frac{Kg}{m^3}$, and a fluid velocity v of 30mph, Table 5 shows the C$_d$A values for *Bucephalus* and the design iterations:

Vehicle	Drag Force (N)	C$_d$A (m^2)
Iteration 1	4.27	.040
Iteration 2	4.41	.041
Iteration 3	4.09	.038
Bucephalus	5.36	.050

Table 5: Drag Force and C$_d$A Values for Candidate Fairings. Note that every iteration improves on *Bucephalus's* drag force and C$_d$A by about 20%.

All of our new designs significantly improve on *Bucephalus's* fairing. The worst potential fairing still results in a 20% better C$_d$A and a smaller stagnation area behind the vehicle at race speeds. Adding a wheel box as in Iteration 3 improves the drag force from our baseline fairing by about 5%. However, before deciding on a fairing shape we analyzed crosswind performance to see how side forces and flow trajectories could impact performance.

In the second simulation, we added a crosswind to simulate possible race conditions, primarily to see how the flow trajectories would manifest themselves on the rear of the vehicle. Since the fairings were primarily designed with forward aerodynamics in mind, the crosswind trajectories should exhibit turbulence and instabilities. We want a fairing that will perform best given a crosswind, an expected weather pattern at a large, open racetrack. As shown in Figure 12, Iteration 3 exhibits less turbulence and looser flow spirals than *Bucephalus.* The other iterations were excluded because they were not materially different than the flow curves shown for Iteration 3.
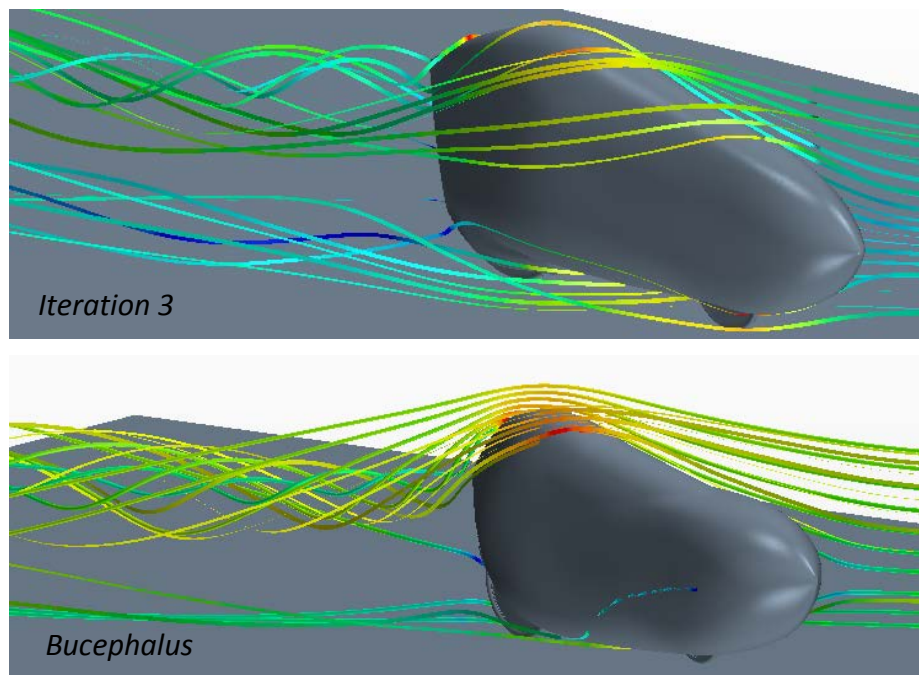

Iteration 3

Bucephalus

Figure 12: Crosswind Velocity Flow Profiles for Iteration 3 and *Bucephalus*. Note that *Bucephalus* experiences more intense turbulent flow from the applied crosswind.

In combination with the flow curves, we took data on the side force exerted by the 10.4mph crosswind. Assuming an overall weight of 230lbs (150lb rider, 80lb vehicle), we found that the side force amounted to about 10% of the

composite weight of the vehicle. Taking into account the crosswind on the course last year, we feel that the side force was manageable and would not result in any stability problems. While riding *Bucephalus* last year in similar conditions, we felt that the wind did not make it uncontrollable.

After performing analysis and examining our C_dA values, we decided to move forward with our Iteration 3 shape. Due to the combination of a low drag force and C_dA, reasonable side force, and minimally turbulent crosswind flow curves, we feel that this fairing gives us the best overall aerodynamic advantage.
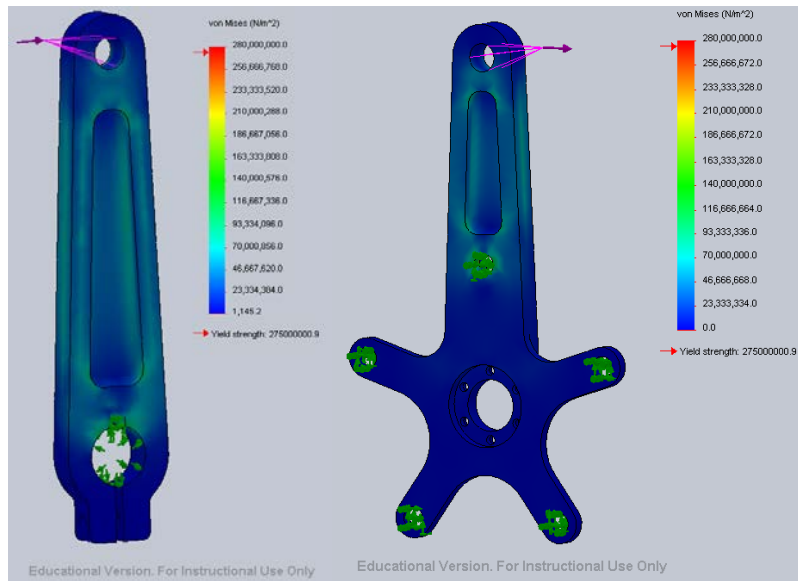
Custom Crank Analysis

Figure 13: FEA analysis of the Custom Crank. An external, static load of 150 lbs is placed remotely from the center of the pedal. The stress within the crank is well below yield, with a minimum FOS of 2.

We verified the integrity of our custom manufactured cranks using the SolidWorks Simulation Finite Elemental Analysis (FEA) package. A static analysis of the crank was determined to be sufficient to determine potential failure.

To simulate the maximum load a crank could undergo, a 150lb force was applied on the center of the pedal. This force is appropriate because it is comparable to a rider standing on the crank, the maximum force a rider would exert on the pedal through the stroke. This load is transmitted to the surface of the pedal hole, where the shaft would be inserted into the crank. The hole of the crankshaft is fixed into position via the key slot.

The factor of safety for the key was calculated to be 2.19 for the static load of 150lbs. In reality, the factor of safety is even greater because the key does not transfer all of the torque from the crank to the shaft. Because the crank is tightly clamped around the shaft, the friction between the two components allows some of the load to be delivered to the crank without stressing the key.

With this loading and fixture setup, Figure 13 shows the internal stresses throughout the crank. As expected, the highest stress is located along the pocket of the crank. Under this maximum loading condition, the crank has a minimum factor of safety of 2. This analysis justifies the crank as functional for *Shadowfax* and not a concern of failure.

Roll Bar Analysis

In accordance with the rules for the 2011 HPVC, we analyzed two static cases of roll bar loading with the SolidWorks FEA package. We also verified these cases with experimental load testing in *Roll Bar Testing.*

The first loading case is a 300lb load applied horizontally to the roll bar at rider shoulder height with a maximum allowable deflection of 1.5in, simulating the vehicle in a side crash. For this simulation, the load is applied to one side of the roll bar. The other side is fixed, as if the bar is resting on the ground. We found that the von Mises stress (as seen in

Figure 14) of the roll bar is significantly under the yield strength of the material, and the maximum displacement is 0.24in. We are therefore confident that the roll bar will meet the safety rating and protect a rider in the event of a fall on the side.
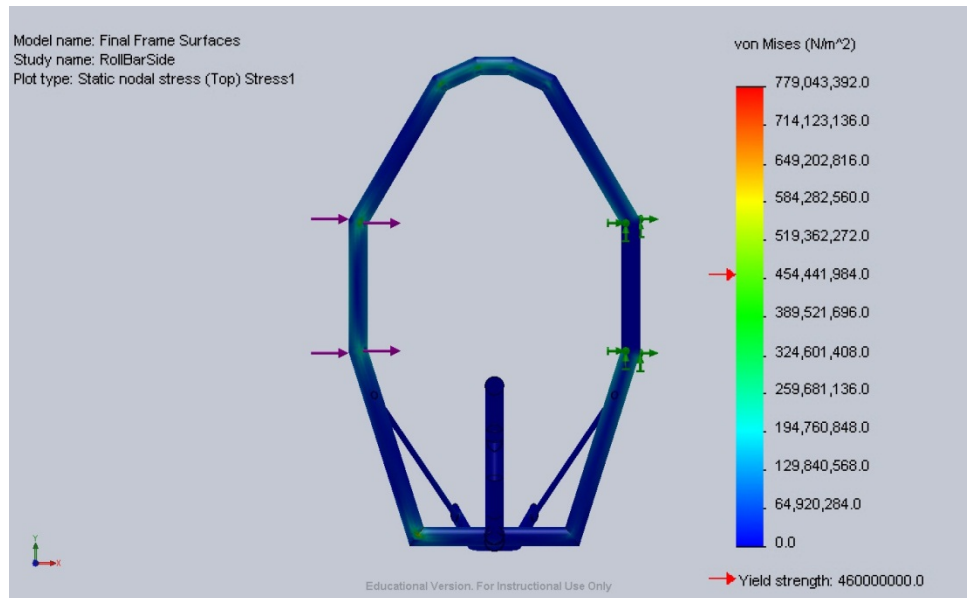

Figure 14: Roll Bar Side Loading FEA. The effective von Mises stress is well below the yield strength for most of the roll bar, thus predicting that the roll bar will be strong enough under side loading. The unrealistically high stress concentrations at the weld joints are computational anomalies due to the perfectly sharp geometry. In reality, the weld bead distributes this stress.

The second case is a 600lb load applied 12° from vertical with a maximum allowable deflection of 2.0in. We applied this loading condition with a fixed boundary condition placed on the head tube and rear fork prongs. This loading condition therefore analyzes both the roll bar and the connecting frame.
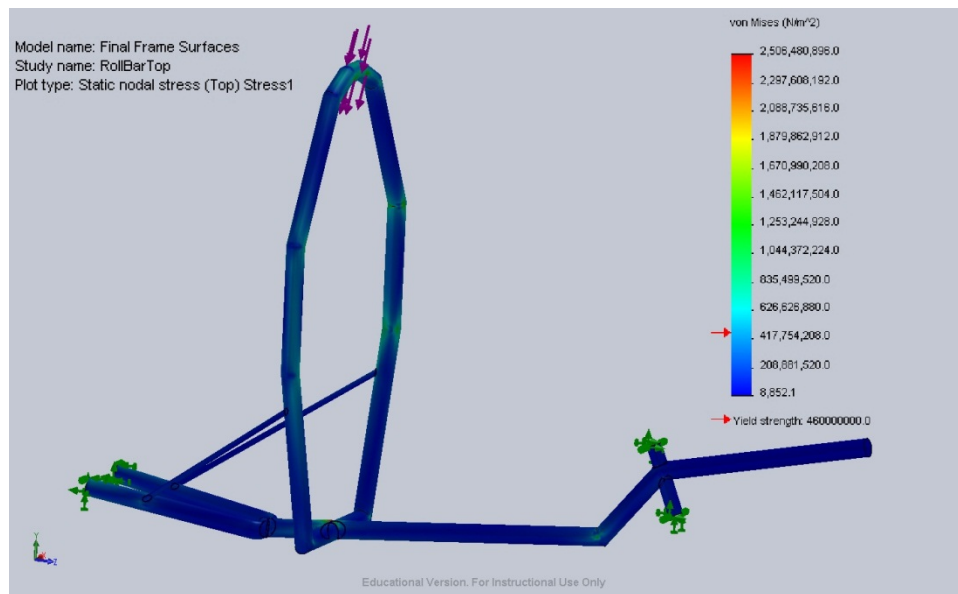

Figure 15: Roll Bar Equivalent von Mises Stress Using SolidWorks Simulation. Shown is the vertical loading case of 600 lb applied at the top of the roll bar, 12 degrees from vertical. The frame is fixed where the frame connects to the wheel at the head tube and the end of the fork.

The effective von Mises stress is again below the yield strength of 460MPa for most of the roll bar (as seen in Figure 15). As expected, the main stress concentrations are seen along the roll bar along the top, where the load is being applied, and along the weld joints. The area of higher stress where the load is applied is due to the unrealistic loading geometry, and is therefore not of great concern. Similar to the side loading condition, the higher areas of stress at the weld joints

is due to the perfectly sharp joints in the simulated vehicle geometry. In reality, there is a more graceful stress distribution due to the weld bead, which is below the yield strength.
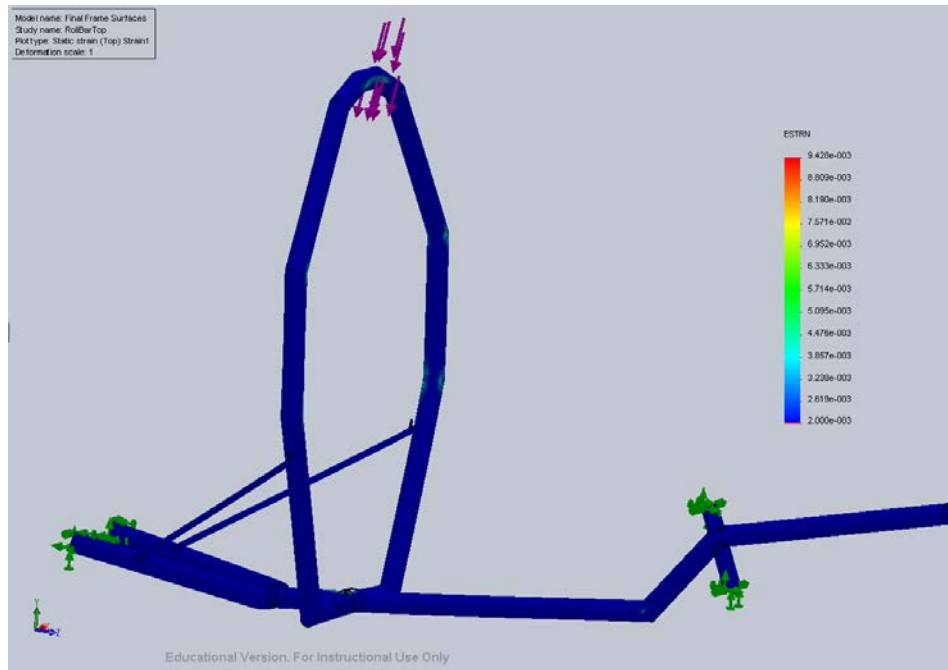

Figure 16: Effective Strain of Roll Bar Under Top Loading. Dark blue areas are under 2% strain, indicating that the material is still in the plastic regime and will not result in fracture. The areas of greater than 2% strain are concentrated at the roll bar joints where the FEA is unrealistic.

Considering that the roll bar is a safety device and is not to be designed for continuous loading, as long as the roll bar does not fracture or deform significantly, the rider will still be protected. The areas of concern where the stress is above the yield strength and the strain is beyond the plastic regime (ε=.02) can be attributed to the effect of tube discontinuities in the SolidWorks model. In reality, these regions of concern are much smaller. Given this, in the regions where the von Mises stress is above the yield strength it is still well below the ultimate strength and thus will not feel.

The maximum deformation from this simulated case is 1.406 inches at the top of the roll bar where the load is being applied, which is within the 2.0 allowable inches. This does not take into account that the fairing will also be structural and will help distribute the load and deformation.

We were confident enough in the results of this FEA to implement this roll bar design. In order to further increase the factor of safety, we would have to change the geometry of the roll bar by either adding more tubes or making the tubes larger diameter. These options trade off additional factor of safety for decreased frontal area decreased weight of the vehicle. Because we were also experimentally testing the roll bar structure, we were confident that the rider safety was not going to be compromised.

In the unlikely event that we observe roll bar yielding or failure before competition, we have budgeted for enough time to re-design and re-fabricate the roll bar during fairing fabrication if necessary. When testing and after any major crashes, we will examine the roll bar to ensure that there is no evidence of extreme deformation or cracking and then discontinue use of the vehicle if appropriate.

Lean Angle Analysis

One issue we experienced last year was contact of *Bucephalus's* fairing with the ground around fast, tight turns. Bottoming out the fairing lifted the rear wheel, causing loss of traction and a subsequent wreck. *Bucephalus's* fairing expanded farther than expected in its lower sections, making the sharp cornering impossible. To prevent this issue from recurring, we designed *Shadowfax's* fairing such that the bike could be tilted to the frictional limit of the tires without rubbing, so that the wheel will slip before the fairing hits the ground.

To determine the allowable tilt, we modeled the bike as a rigid bar with its mass concentrated about a single point, as depicted in Figure 17. The maximum steering angle can be calculated by summing the moments about the center of mass.
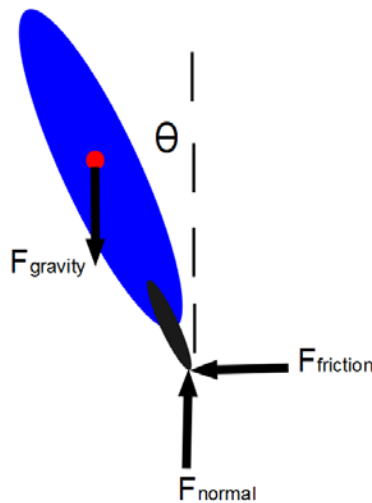

Figure 17: Rigid Bar Approximation

It can be shown that $\theta_{max} = \arctan(\mu)$, where θ_{max} is the maximum lean angle of the vehicle and μ is the coefficient of friction between the ground and the tire. A reasonable estimate for μ is 0.85 [4]. Based on this value, the steepest angle the bike could possibly lean on flat ground before arriving at the frictional limit of the tire is approximately 40˚. Thus, we made sure that our fairing would not intersect the ground, as shown in Figure 18.
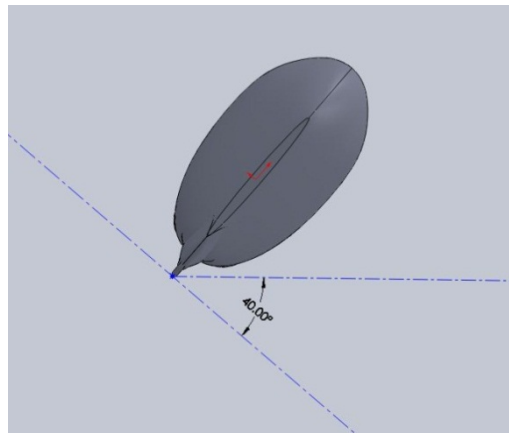

Figure 18: Fairing at Maximum Tilt Angle. Note our fairing does not contact the ground at 40°.

With this analysis and our improved fairing fabrication methods, *Shadowfax*'s fairing should not make undesired contact with the ground on sharp turns, and we should have fewer crashes.

Effect of Drag and Weight on Speed

Compared to the other teams' competition vehicles last year, *Bucephalus* had both a larger frontal area and a larger weight. Before designing *Shadowfax*, we created a model of a vehicle to compare gains from weight savings with the gains of aerodynamics savings. Based on the results of this model, we were better able to direct our design efforts in order to maximize our time savings.

Our model determined to what extent the mass of the vehicle and the C$_d$A (the drag coefficient multiplied over the cross-sectional area of the fairing) affect the bike in both the endurance and the sprint races. In the model, we assumed the only two forces on the bike were the drag and the force the rider outputs. We also assumed that the rider output a constant power, so that the force the rider exerts on the bike is equal to the output power of the rider divided by

velocity. A third assumption we made was that for bike speeds lower than the threshold velocity at which a rider can spin freely, the rider outputs a constant force equal to the force output at the threshold velocity. The drag coefficient we used was determined using the simulations from the previous year's fairing. The results we found are displayed in Figure 19 and Figure 20.
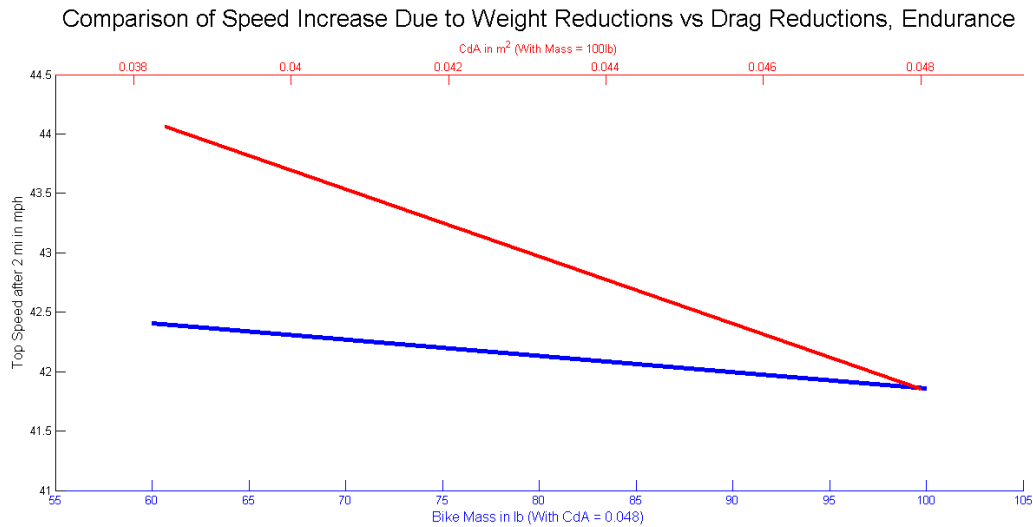

Figure 19: Comparison of Speed with Respect to Weight and Drag Reductions (Endurance). The top speed of the vehicle after it has gone two miles (and had sufficient time to accelerate) is dramatically affected by a change in the C_dA, but not significantly by a change in mass.
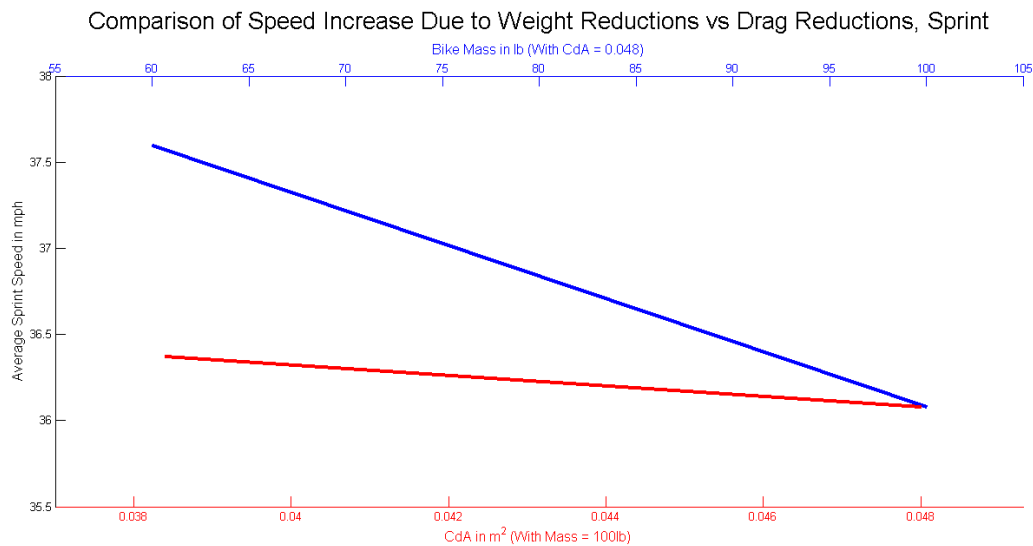
Figure 20: Comparison of Speed with Respect to Weight and Drag Reductions (Sprint). The average speed during the sprint race is significantly affected by vehicle mass, but not by the C_dA.

Our results show that the drag coefficient of the fairing greatly impacts the top speed seen over a longer course, whereas a lighter mass improves top speed of a sprint race. Our goal, therefore, is to minimize our C_dA while aiming for a fairing which is as light as possible.

Weight Comparison Analysis

Measuring the weight of various sections of *Bucephalus* showed that there are significant areas of opportunity to decrease weight on *Shadowfax*. *Bucephalus's* weight distribution is displayed in Figure 21. The fairing itself weighed about 19.5kg (43lbs.), which is approximately 45% of Bucephalus' weight without the rider. This presented a major area

for potential weight savings. In addition, the window was constructed of a heavy thick polycarbonate. To address these areas, this year's fairing is made of vacuum-bagged carbon fiber with a thin polycarbonate window. We can also reduce weight in the seat. By moving from a wooden seat to a hammock style seat, we save 3lbs, a 42% reduction. Although this reduction in weight is not significant compared to the reduction in weight of the fairing, the decrease in the weight still contributes to a lighter vehicle this year.
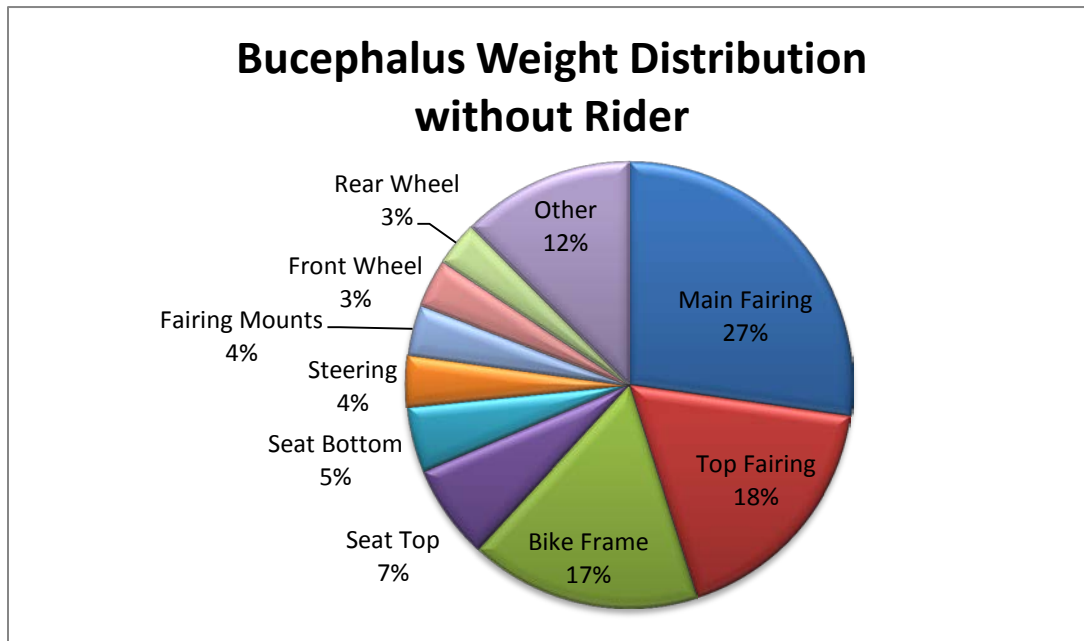

Figure 21: Displays the weight distribution of 2010 vehicle *Bucephalus*. This data was used primarily to determine areas of weight reduction opportunity for *Shadowfax*.

Human Error Analysis

Human error caused significant time loss in the endurance competition last year. We experienced nine separate incidents, including crashes, flat tires, and black flags, that lost us distance on the track. In addition, there was a noticeable trend that the laps immediately following a crash were slower, likely due to the riders losing confidence. To quantify these losses, we looked at the raw lap time data from last year's HPVC East competition. We averaged the lap time for each rider's laps without incident to get a baseline ideal speed, and used that figure to extract the time lost to crashes and other human errors. We found that, in total, we lost 15 minutes 22 seconds. Given that our average was 1:49 per lap, we lost 8.5 laps of travel due to human error. In order to minimize this error during this year's endurance event, we will implement a more rigorous training program to ensure that all riders are confident riding with the fairing and able to navigate potential course hazards.

Testing
Developmental Testing

This year, we had the option of fabricating our fairing using either carbon fiber or fiberglass. To form a basis for our decision, we performed three point bend testing on our material samples. Since our fairing will primarily experience bending during accidents, a fairing material which provides the greatest flexural strength for the lowest weight is ideal. If a fairing of each material were made to have equal strengths, the one made from a higher specific strength material will be lighter.

The results of our tests can be seen in Figure 22. Vacuum-bagged carbon fiber has the highest flexural modulus and ultimate strength, making it an optimal option for fairing material. Carbon fiber laid up with standard (non-vacuum-bagged) practices traps epoxy between the layers of fiber. Because the carbon matrix is considerably less permeable than the fiberglass, the difference in strengths of standard and vacuum-bagged carbon fiber is greater than that of

standard and vacuum-bagged fiberglass. In fact, standard fiberglass is stronger than vacuum-bagged fiberglass in bending because the fiberglass benefits from a layer of hard yet brittle epoxy.
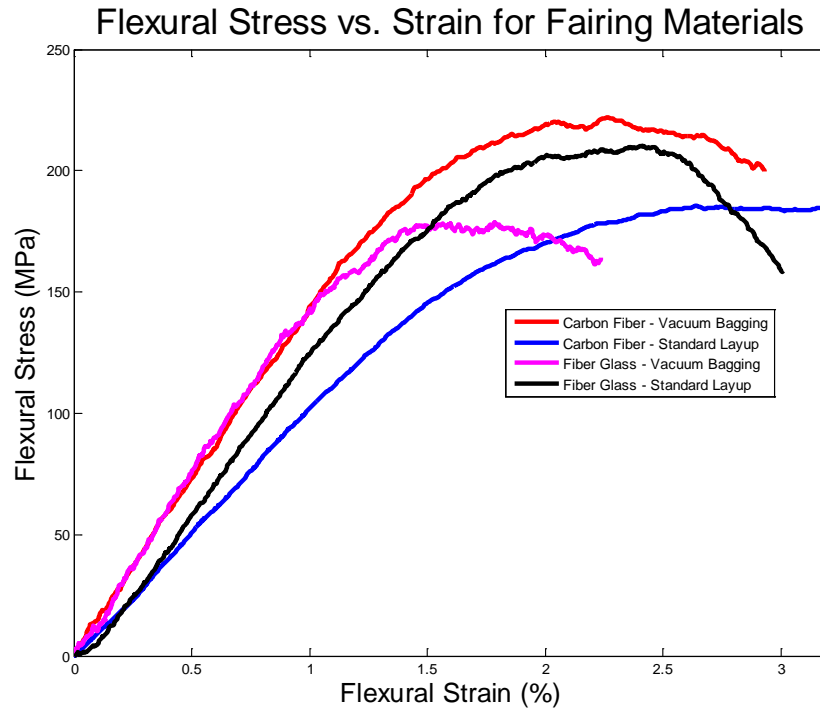

Figure 22: Flexural Stress-Strain Relationship of Fairing Materials. Note that vacuum-bagged carbon fiber has both the highest ultimate flexural strength and flexural modulus. Testing used 2in by 4in samples on the three-point bend fixture in an Instron.

Based on our tests, we calculated the specific flexural strengths for each material as seen in Table 6. We opted to use vacuum-bagged carbon fiber as it has the highest flexural modulus and the highest ultimate strength. We will perform a layup with two layers of vacuum-bagged uni-directional carbon fiber and will insert ribs as needed.

Material	Max Flexural Stress (MPa)	Density (kg/m³)	Specific Flexural Strength (kN*m/kg)
Standard Carbon	185.41	1041.30	178.06
Vacuum Bagged Carbon	**222.15**	**1123.85**	**197.67**
Standard Fiberglass	210.32	1118.09	188.11
Vacuum Bagged Fiberglass	178.71	1169.61	152.79

Table 6: Strength to Weight Comparisons of Fairing Materials. Vacuum-bagged carbon has the lightest specific flexural strength, or strength to density ratio. Using vacuum-bagged carbon allows us to make the lightest fairing for a necessary strength.

Performance Testing

Drivetrain Performance Testing

Shadowfax's drivetrain design is entirely different from last year's race bike, *Bucephalus*. Unlike *Bucephalus*, *Shadowfax* is rear-wheel drive, has a custom bottom bracket, and was built using a frame jig to precisely align drivetrain components before welding. These changes were in response to several perceived problems with previous vehicles. First, *Bucephalus's* nosecone had to be slightly wider to allow for the typical crank and bottom bracket width, making the fairing less aerodynamically efficient. Second, the front-wheel drivetrain was somewhat unwieldy, as it was uncomfortably close to the rider's knees and the chain interfered with the front fork on harsh turns. Finally, the slight frame misalignments in all our previous vehicles made it impossible ensure chain reliability without resorting to chain guides.

Our primary goal in the new drivetrain design was to surpass *Bucephalus's* measured 95% drivetrain efficiency with our drivetrain changes. We had previously achieved 95% efficiency in rear-wheel drive vehicles, overcoming the classic problem of efficiently routing the chain to the rear wheel. We had never made a custom bottom bracket before, and we were unsure if our frame jig made a measurable improvement on the drivetrain efficiency. Unfortunately, at the time of this testing, the *Shadowfax* drivetrain was not in testing condition, so the almost identical *Bilius* prototype drivetrain was tested instead.
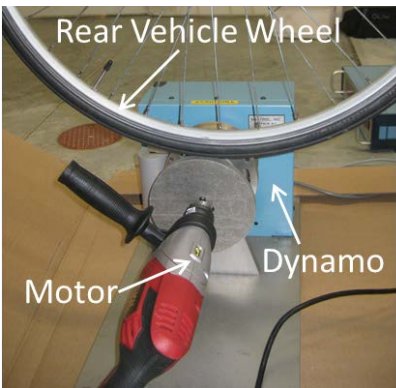

Figure 23: Drivetrain Efficiency Setup. The vehicle drivetrain is driven backwards from the wheel, and the torque required to do so at riding speeds is recorded. The dynamo disc is sized such that the effective groundspeed is roughly 20mph.

We tested the *Bilius* prototype drivetrain with the same technique as last year, using a motor as a constant power source. We placed the vehicle's wheel on the rotating disc of a dynamo-motor setup (Figure 23). We ran the motor at a constant voltage and recorded the speed using a dynamometer. Next, we removed the vehicle and ran the motor at the same voltage, which yielded a faster speed because there was no friction from the drivetrain to slow it down. We then applied the dynamo brake until the dynamo ran at the same speed as when the drivetrain was attached, which necessarily meant that the torque from the brake equaled the frictional torque from the bike. We then recorded the frictional torque and calculated the efficiency (Figure 24).

That setup was a reasonable approximation for the actual riding efficiency because it included both the wheel contact friction and the entire drivetrain viscous friction. It did, however, ignore several factors, including the static startup friction and frictional forces in the unpowered front wheel. It also makes the assumption that the drivetrain will have the same performance if powered backwards from the wheel as if it is powered from the pedals. This effect is largely mitigated by running the motor rotationally backwards, thereby ensure that the correct chain lines are tensioned.

Gear Ratio	Disc RPM	Torque Loss (oz-in)	Power Loss (W)	Pedal RPM	Efficiency (%)
Bilius **Prototype 2011 (Rear Wheel Drive)**					
2.04:1	950	13.8	9.69	106.42	**96.60**
2.68:1	934	17.3	11.95	79.71	**95.81**
3.58:1	916	18.8	12.73	58.63	**95.53**
Bucephalus **2010 (Front Wheel Drive)**					
4.55:1	880	30.4	19.78	77.36	**93.06**
6.83:1	887	21.9	14.36	51.99	**94.96**
9.01:1	890	16.9	11.12	39.12	**96.10**
Prototype 2010 (Front Wheel Drive)					
5.54:1	889	17.5	11.50	64.16	**95.96**
7.13:1	880	28.5	18.55	49.40	**93.49**

After testing, we found the *Bilius* prototype was an average of 96% efficient over its three different gears, which is a 1% improvement over last year that can likely be attributed to our new frame jigging technique. Unfortunately, even though these measurements are certainly well correlated with known phenomena that affect the drivetrain efficiency, the shortfalls of our methodology make our quantitative results somewhat suspect. The *Bilius* prototype is probably not exactly 96% efficient. However, this analysis is a powerful *comparative* tool for ensuring drivetrain quality in relationship to previous vehicles, since all our previous vehicles have been tested in precisely the same way. We can therefore conclusively say that as long as these shortcomings are consistent across all our vehicles and all of our testing, then the *Bilius* drivetrain is on par or better than our previous vehicles.

Fairing Flow Testing

Along with the CFD analysis of our fairing shape, we were curious about the airflow over the actual fairing. One common way of observing laminar or turbulent flow over a surface is to attach yarn tufts to the surface as indicators. Areas of non-desirable flow are indicated by where the two tails of the yarn are pointing in different directions or where the yarn tails are pointing opposed to the direction of bike movement, which is characteristic of turbulent flow. By looking at the transition from regular to irregular yarn, we can estimate where the flow transitions from laminar to turbulent flow and compare this to the CFD predictions. If the yarn tufts are separated, they indicate an increase in wake and thus an increase in undesirable drag.

Eight-inch long pieces of yarn were taped to *Bucephalus* to validate the previous fairing model. Olin does not have access to a large wind tunnel or other suitable flow testing equipment, so testing was completed by having a team member ride the vehicle. As the rider moved at 15mph, still photos were taken for later analysis, as seen in Figure 25.

Figure 25: Yarn Tuft Testing. The disturbances in the white yarn show the flow over the fairing surface.

The yarn indicates a very smooth profile over the front two thirds of the fairing. Around the rear wheel cover, there is an eddy indicated by the yarn pointing forward. Based on this and the fact that some of the yarn tuft pairings are pointing different ways, we believe that the airflow turns turbulent aft of the roll bar at the maximum width of the bike. This is consistent with our new CFD analysis technique, indicating that the CFD is a reasonable prediction of the flow around our fairing.

Steering Geometry Testing

We designed our steering geometry on the prototype to have several variable components to gain a better understanding of how the steering parameters of rake, tiller, and nonlinearity affect the ridability of the bike. When we initially swept through the range of parameters we created, we found that we were not able to build an unridable configuration even when using extreme parameters.   Since the differences in handling were slight, we created a series of tests to pinpoint how changes in steering geometry affected bike stability.

Definition of parameters

The three parameters we could alter directly were the steering type, the rake, and the tiller. We tested two types of steering: linear and nonlinear, further discussed in *Nonlinear Steering Design*. To test different settings for rake, we attached a special bracket with four mounting points for the front wheel to the fork. Traditionally the axle is slightly

forward of the steering axis, which we noted as positive rake. We could also flip the bracket backwards to test negative rake (Figure 26). Finally, we could test the tiller, the length from the handlebars to the steering column. For the purposes of this section, the tiller number refers to the tiller length in 1¾" increments, and the rake number is the rake length in ¾" increments.
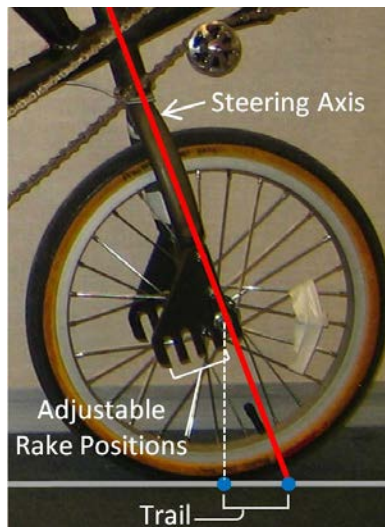

Figure 26: Adjustable Rake Fork. The custom plate where the wheel is mounted allows for testing seven different rake configurations. The bike is currently shown at zero rake and the plate mounted for testing negative rakes. The plate can be flipped such that the dropouts are forward of the fork in order to test positive rake.

Variations in Maneuverability

Our primary goal in designing the steering stability is to increase rider confidence, which allows for more assertive riding and thus faster racing times. Rather than trying to measure the stability in a direct way, we decided to measure the rider sprint times around a test loop for a variety of parameters.

Initially, we hoped to test the steering stability on a long course that simulated racing conditions. However, we found that the effect of fatigue masked any distinction that might have existed between steering parameters. We observed this through testing of four configurations with multiple trials of three riders each, including comparisons over multiple days. From this, we concluded that steering parameters do not have a noticeable effect on endurance riding, but are likely more important in rapid, low speed maneuvering necessary for safe riding in a race setting.

In an attempt to separate fatigue from the data, we laid out a short 150m figure eight loop with two 5m radius curves on the end to simulate the minimum course turning radius. It also features a section with 4 cones spaced 10m apart for slaloming to simulate navigating through traffic. Each trial consisted of three loops. After running 9 trials over the course of 3 hours, our riders were not fatigued and were able to post the same times at the beginning and end of testing on our control bike.

We accounted for different rider speeds by taking the difference between each trial time and the given rider's average. The results from this can be found in Table 7. The maximum difference is only 4%, which is not a significant difference considering our measurement inaccuracies. This independently confirmed that there is little efficiency difference between different steering parameters, and we can readily adjust to whatever geometry we desire. Within the data collected, the variations that do exist are consistent with what we would expect. For instance, the extreme rake positions of 3 and -3 are slower than other rake positions. This leads us to believe that our time distributions are not completely arbitrary, that the bike is more ridable with a rake of 0 or -1, and that nonlinear steering does not improve handling.

Steering Parameters	Time Difference, Seconds
Linear Steering, Rake 3, Tiller 3	2.75
Linear Steering, Rake 1, Tiller 3	0.333333
Linear Steering, Rake 0, Tiller 3	-1.5
Linear Steering, Rake -1, Tiller 3	-1.66667
Linear Steering, Rake -3, Tiller 3	1.25
Linear Steering, Rake 0, Tiller 1	-1.75
Nonlinear Steering, Rake 0, Tiller 3	1.25
Nonlinear Steering, Rake -1, Tiller 3	-1.33333

Table 7: Average time difference from rider averages for obstacle course. The combined average time over five riders and 37 runs was 72 seconds. Note that overall tiller 3 and rake 0 or -1 are the best configurations.

Qualitative Observations

When running the quantitative testing, the riders also commented on the vehicle handling during the trials. Two configurations consistently made the rider less confident. With rake 3 and tiller 3, riders reported that the steering felt "sharper" and that the vehicle tried to come "out from under" the rider while leaning into tight turns at low speed. Nonlinear steering with rake 0 and tiller 3 gave riders trouble on tight corners, although taking wider corners at higher speeds was comfortable. The other nonlinear setting felt better, but riders still reported an entirely different, non-intuitive feel to the steering. For the set of trials with tiller 1, riders reported twitchy steering at both high and low speeds. In comparison, rider responses to trials with tiller 3 and rake around zero were either positive or indifferent, mostly reporting that the bike felt much like other recumbent bicycles. Riders reported feeling the most comfortable with a setting of rake 1 and tiller 3, which is not surprising considering this is the closest to a standard set up and also very similar to the other bikes our team has built in the past. The one intriguing piece of data is that riders reported that rake -1 and tiller 3 was stable and comfortable at high speeds and in long turns.

We also compared the learning rate for new riders trying both linear and nonlinear. Each year, our school holds a series of club fairs where prospective students have a chance to ride the vehicles. On the first two weekends, we gave the prospective students the option to ride *Bilius* with linear steering, and on the third we switched to nonlinear. We used a constant rake of 0 and the tiller of 3 for all weekends. We estimate that at least 10 riders learned how to ride *Bilius* in each configuration. Based on the observations of the team members who were helping the prospective students learn, there was a steeper learning curve with the nonlinear steering. This correlates with our observation that nonlinear steering is less intuitive at low speeds, and is therefore less desirable for learning.

Roll Bar Testing

As per ASME safety rules, we performed load testing on the final roll bar in addition to FEA analysis. Because our campus only has a small Instron tensile tester available, conducting any testing on the roll bar with this machine was not possible because there is no way available to fix *Shadowfax* into the test apparatus. Thus, we manually loaded the roll bar with dumbbell weights suspended on a wood platform. The FEA predicted a 1.4in maximum displacement of the roll bar under top loading, and a 0.24in displacement under side loading. We measured the height of the roll bar before, during, and after each loading in order to measure the deflection and determine if the deformation was elastic. We measure the top displacement along the Z axis of the bike to be 1in in top loading and the displacement along the X axis of the bike to be 0.25in in the side loading. These numbers are consistent with the predicted values and thus both below the allowable deflections.

Figure 27: Vertical load testing. 600lbf was suspended 12° from vertical. The roll bar successfully passed the loading test and only displaced elastically under load. The team members pictured are applying negligible horizontal forces to balance the vehicle.

For the vertical load test, *Shadowfax* was tilted until the wheelbase was 12° off the horizontal in order to ensure that the vehicle could withstand critical moments. We then placed 600lbf on a platform suspended from the top of the roll bar (Figure 27) as dictated in the rules. The roll bar expanded at the corners in the horizontal direction and tilted backwards, but both displacements were under the 2.0in maximum allowable deflection, verifying our computational results. After loading, the roll bar returned to its original shape and original height as measured before and after testing with no visible damage to the structural integrity, indicating that the roll bar deformation was within the elastic region on the stress strain curve for steel. The success of this test confirms our conclusion in the roll bar analysis section that the stresses shown above the yield stress were a function of the uncertainties of FEA and not a weakness in our design.
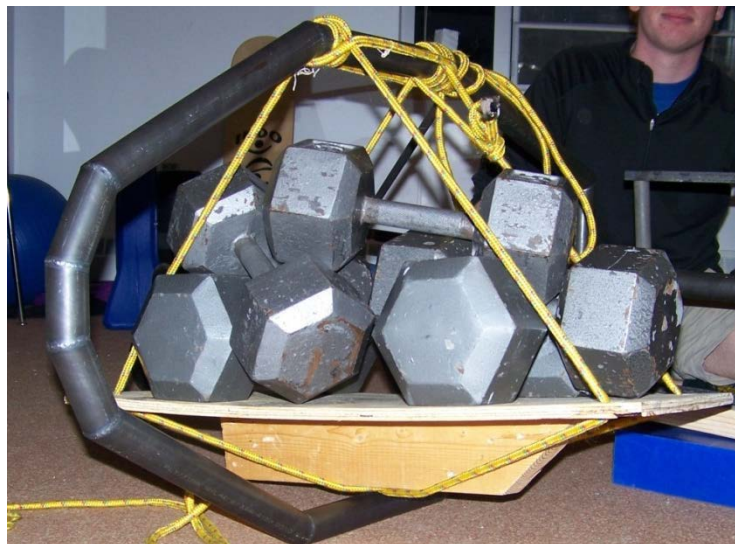
Figure 28: Horizontal load testing. 300lbf were suspended at shoulder height. The roll bar again passed the loading test and only displaced elastically under load.

To test the side loading, we placed the bike on its side and hung 300lbf at shoulder height (Figure 28). The measured displacement due to loading was 0.25in and the roll bar returned to its original measured height once unloaded. These results were once again well within the allowed displacement and consistent with the FEA.

Turning Radius Comparison

During steering testing, we completed time trials on the Olin College campus. Once the race course was posted, we were able to compare our course to the course we will ride at competition for the endurance event (Figure 29). Specifically looking at the corners indicated that the Olin test course was very similar to the published endurance course at Indianapolis Motor Speedway, so we feel the data was collected under good testing conditions.
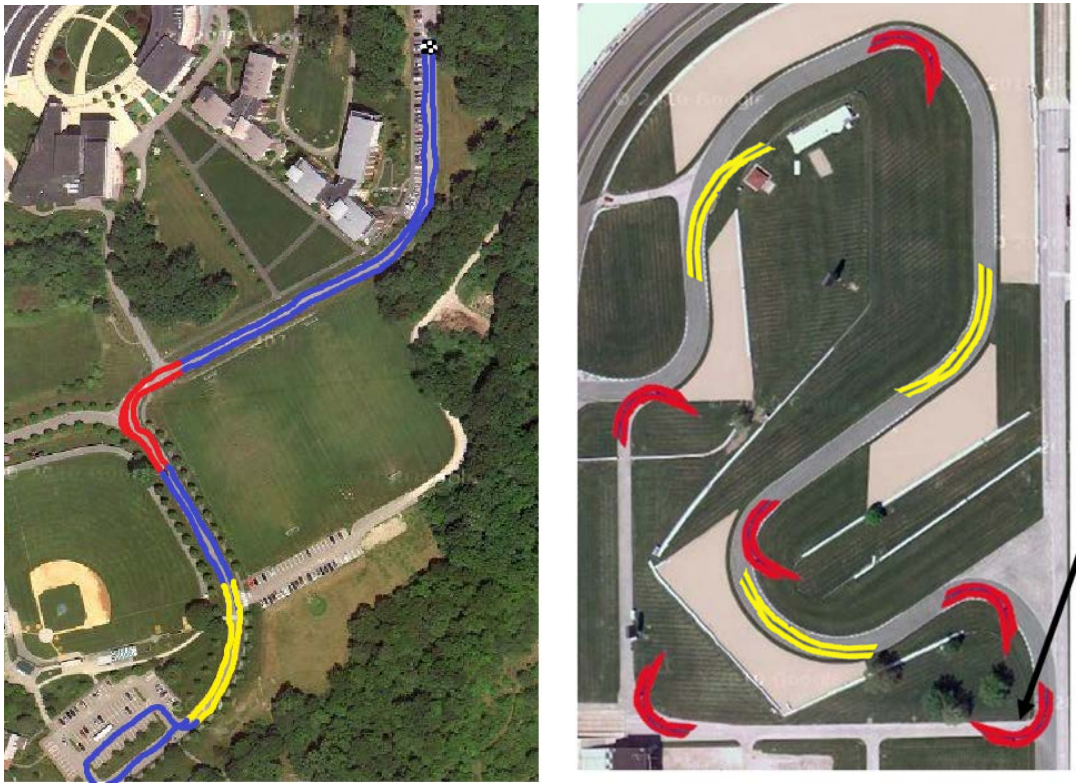

Figure 29: Olin Testing Course (left) vs. IMS Endurance Course (right) – The red and yellow corners are a scale projection of the corners ridden at Olin during testing. The indicated gap (black arrow) shows the only corner that we predict to not be able to ride at full speed.

Safety

Shadowfax has been designed to provide an environment of safety for the rider and all bystanders. Ideally, our focus on increasing vehicle stability and focus on rider fit will give the riders increased confidence and visibility and serve as a preventative measure for crashes. In the event that a crash does occur, our vehicle is also constructed to protect the rider from injury.

Our previous vehicles have consistently struggled with the braking safety test. Also, the rain and oil that it raised from the track during the drag event at the 2010 HPV East Competition further reduced our braking force. To avoid this dangerous situation again, we upgraded from a single caliper brake on the front wheel to dual disc brakes. This increases our theoretical maximum braking force, better protects the braking surfaces from contamination, and provides a redundant system in the event of a failure.

In the event of a crash, the vehicle features a full fairing to protect the rider from abrasion, a roll bar that meets top and side loading requirements, and a four-point automotive performance seat belt that is easily adjustable to fit riders of all shapes and secure the rider within the protection system.

Because the steering system is located in close proximity to the rider's legs and chest, we have optimized the handle bar shape from a U shape to a V shape to reduce contact with rider thighs and ensured that it contains no open tube ends.

In the past, there has been a safety hazard with the interior of the fairing scratching riders from frayed fiberglass that became sharp after the epoxy layup. By vacuum bagging the fairing with a male mold, the inside should be much smoother and thus safer.

Shadowfax's biggest safety risk comes from the fact that it is designed for the speed class, and therefore the design does not include a means for the rider to support himself after he slows to a stop. Thus, if a rider were to stop outside of the pit, he would likely fall over and could be an obstruction to other vehicles on the course. In the past, the team has ensured that team members are all around the course to recover riders in the event of a crash, and we intend to continue this successful policy.
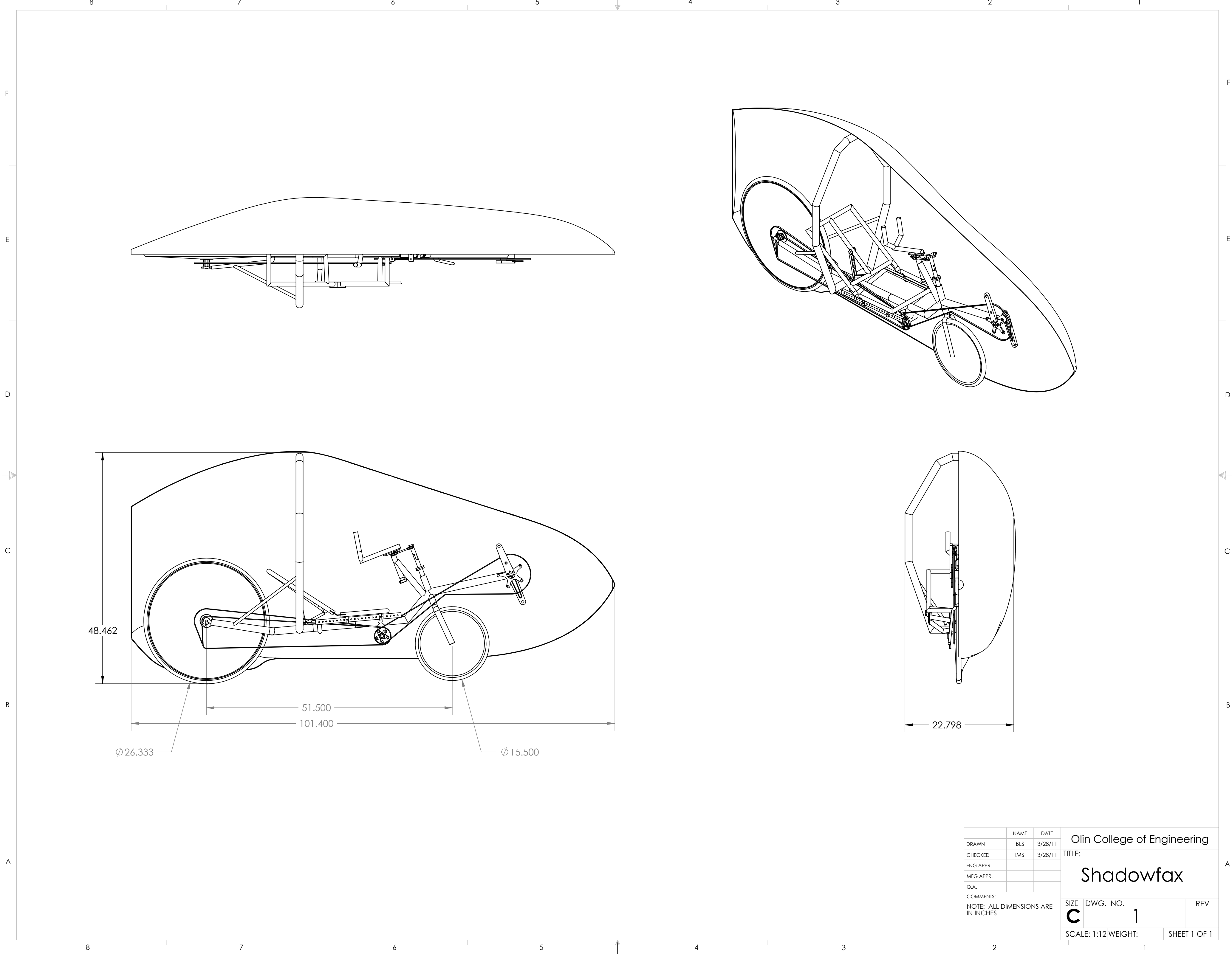
Appendix 1: Costs

Single Vehicle Cost Estimation

Description	Qty	Unit Cost	Units	Total
Frame				
Thin Walled 4130 Steel Tubing	18.0	$3.40	Per Foot	$61.20
Welding Supplies	1.0	$20.00	Lump Sum	$20.00
Assorted Mounting Hardware	1.0	$60.00	Lump Sum	$60.00
			Subtotal	**$141.20**
Fairing				
Epoxy	2.0	$60.00	Per Gallon	$120.00
Carbon Fiber Cloth	15.0	$8.40	Per Yard	$126.00
Assorted Composites Tools	1.0	$50.00	Lump Sum	$50.00
Blue Foam (2' x 8')	26.0	$14.35	Per Sheet	$373.10
acuum Bagging Supplies	1.0	$122.00	Lump Sum	$122.00
Vacuum Pump	1.0	$110.00	Per Pump	$110.00
PETG (4' x 8')	1.0	$36.82	Per Sheet	$36.82
Coroplast (4' x 8')	0.5	$20.00	Per Sheet	$10.00
			Subtotal	**$947.92**
Drivetrain				
Derailer	1.0	$50.00	Per Unit	$50.00
Wheels	2.0	$100.00	Per Wheel	$200.00
Crankshaft Steel	1.0	$15.00	Per Unit	$15.00
Bottom Bracket	2.0	$25.00	Per Unit	$50.00
Crank Aluminum	1.0	$15.00	Per Unit	$15.00
Chains	2.0	$20.00	Per Unit	$40.00
Interchange Sprockets	2.0	$15.00	Per Unit	$30.00
Pedals	1.0	$35.00	Per Set	$35.00
Disc Brakes	2.0	$50.00	Per Set	$100.00
			Subtotal	**$535.00**
Seat				
Nylon Webbing	50.0	$0.52	Per Foot	$26.00
Thin Walled Steel Tubing	6.0	$2.25	Per Foot	$13.50
1/8" Steel Plate (6" x 2')	1.0	$30.00	Per Plate	$30.00
Aluminum Block	1.0	$20.00	Per Block	$20.00
Pins	2.0	$2.00	Per Pin	$4.00
	1.0	$5.00	Lump Sum	$5.00
			Subtotal	**$98.50**
			Total Cost	**$1,722.62**

Multi-Vehicle Estimation

Description	Qty	Unit Cost	Units	Total
Labor Per Month				
Machinist/Welder	3	$3,200.00	Per Month	$9,600.00
Composite Technician	3	$2,080.00	Per Month	$6,240.00
Floor Worker	4	$1,600.00	Per Month	$6,400.00
Manager	1	$4,800.00	Per Month	$4,800.00
			Subtotal	**$27,040.00**
Bike Cost Per Month				
Cost Savings Factor for Bulk Purchase	50%			
Drivetrain Components	10	$267.50	Per Bike	$2,675.00
Frame	10	$70.60	Per Bike	$706.00
Fairing	10	$473.96	Per Bike	$4,739.60
Seat	10	$49.25	Per Bike	$492.50
			Subtotal	**$8,613.10**
Monthly Overhead Costs				
Building Rental		$1,500.00	Per Month	$1,500.00
Utilities		$400.00	Per Month	$400.00
Welder Operating Costs		$20.00	Per Month	$20.00
			Subtotal	**$1,920.00**
			Total Monthly Costs	**$37,573.10**
Equipment (Single Purchase)				
Mill	1	$22,000.00	Initial Purchase	$22,000.00
Lathe	1	$20,000.00	Initial Purchase	$20,000.00
Grinder	1	$150.00	Initial Purchase	$150.00
Welder	1	$3,500.00	Initial Purchase	$3,500.00
Band Saw	1	$2,000.00	Initial Purchase	$2,000.00
Frame Jig	1	$150.00	Lump Sum	$150.00
			Initial Purchase Total	**$47,650.00**
		Cost Per Bike		**$3,823.49**

References

[1] Brown, Sheldon. "Bicycle Cranks." *Sheldon Brown-Bicycle Technical Information*. 18 Sept. 2010. Web. 28 Mar. 2011. <http://www.sheldonbrown.com/cranks.html>.

[2] Wilson, David Gordon, Jim Papadopoulos, and Frank Rowland. Whitt. "Human Power Generation."*Bicycling Science*. Cambridge, MA: MIT, 2004. 87. Print.

[3] Carroll, Douglas R. 2003. *The Winning Solar Car.* Warrendale PA : SAE International, 2003.

[4] Baker, J.S. "Traffic Accident Investigation Manual", 1975.

[5] Dellinger, Dan. "Wind- Average Wind Speed- (MPH)." *National Climatic Data Center*. 20 Aug. 2008. Web. 1 Mar. 2011. <http://lwf.ncdc.noaa.gov/oa/climate/online/ccd/avgwind.html>.

48.462

51.500

101.400

⌀26.333

⌀15.500

22.798

	NAME	DATE
DRAWN	BLS	3/28/11
CHECKED	TMS	3/28/11
ENG APPR.		
MFG APPR.		
Q.A.		
COMMENTS:		

Olin College of Engineering

TITLE:

Shadowfax

NOTE: ALL DIMENSIONS ARE IN INCHES

SIZE	DWG. NO.	REV
C	1	

SCALE: 1:12 WEIGHT: SHEET 1 OF 1